ELSEVIER

Potential role of energetic particle observations in geomagnetic storm forecasting

Dheyaa Ameri *, Eino Valtonen

Department of Physics and Astronomy, University of Turku, 20014 Turku, Finland

Abstract

We have searched for solar proton events consisting of both solar energetic particles (SEPs) accelerated near the Sun and energetic storm particles (ESPs) accelerated by interplanetary shocks driven by coronal mass ejections (CMEs) and observed near the time when the shock passes the observer. The purpose of this study is to investigate the possibilities and advantages of using energetic particle observations for mid-term (warning time several hours) forecasting of geomagnetic storms or as a support for longer-term forecasting methods based on solar observations. The study period extends from May 1996 to December 2017 covering the entire solar cycle 23 and the major part of solar cycle 24. Using two particle energies, 2 and 20 MeV, we found 95 SEP–ESP events of which 65 were associated with geomagnetic storms with Dst $\leqslant -50$ nT caused by CMEs. We performed correlation analysis between $\log_{10}|\text{Dst (nT)}|$ and various parameters characterising the particle events or the associated CMEs. We found the best correlations for the single independent variables $\Delta t_{ESP-SEP}$ ($r = -0.47 \pm 0.08$), which is the difference between the ESP peak time and SEP onset time, the CME direction parameter DP ($r = 0.47 \pm 0.10$), and the logarithm of the maximum ESP energy $\log_{10}[E_{ESP}^{max} \text{ (MeV)}]$ ($r = 0.44 \pm 0.11$). Using a linear combination of these three variables improves the correlation ($r = 0.68 \pm 0.07$). We suggest that an empirical equation based on these three parameters and requiring only coronagraph observations of CMEs and energetic particle measurements in interplanetary space can be used for mid-term forecasting of geomagnetic storm strengths. We found that 74% of the strongest storms (Dst $\leqslant -200$ nT) during the study period were associated with energetic particle events. The average warning time and its standard deviation for all geomagnetic storms associated with SEP–ESP events was (15 ± 10) hours.

1. Introduction

Geomagnetic storms are one manifestation of space weather (Schwenn, 2006; Pulkkinen, 2007). Strongly disturbed magnetoshere can lead to enhanced levels of energetic particles in the radiation belts and increased magnetospheric currents, which can have hazardous effects on the surface of the Earth. Therefore, it would be important to be able to forecast the occurrence and strength of geomagnetic storms.

Many investigations have been performed to find and explain the solar and interplanetary causes of geomagnetic storms (*e.g.*Gosling et al., 1991; Gonzalez et al., 1999; Zhang et al., 2003, 2007a,b; Schwenn et al., 2005; Gonzalez et al., 2011; Richardson and Cane, 2012). It has been established that the basic cause of strong nonrecurrent geomagnetic storms are coronal mass ejections (CMEs) and their interplanetary counterparts (ICMEs) accompanied with different magnetic structures and often driving shocks in interplanetary space. A recent review of

* Corresponding author also at: Department of Ecology, University of Basra, Karmat Ali B.P. 49, Basra, Iraq.

E-mail addresses: dheyaa.a.ameri@utu.fi (D. Ameri), eino.valtonen@utu.fi (E. Valtonen).

the geoeffectiveness of interplanetary shocks driven by solar eruptions was presented by Oliveira and Samsonov (2018). Moderate storms, however, can also be caused by corotating interaction regions of fast and slow solar wind (Echer et al., 2013). It has also been established that the main direct cause of geomagnetic storms is the magnetic reconnection of interplanetary magnetic structures with the Earth's magnetic field transferring mass and momentum into the magnetosphere (*e.g.* Echer et al., 2008, and references therein). The main single factor contributing in the occurrence of magnetic storms is the existence of a strong and long-duration southward magnetic field component in the interplanetary magnetic structure encountering the magnetosphere (Gonzalez et al., 1994; Tsurutani and Gonzalez, 1997).

It is reasonable to expect that halo CMEs occurring on the front side of the Sun are the most geoeffective, *i.e.,* most probably cause strong geomagnetic storms, because the associated ICMEs and shocks have the highest chance of hitting the Earth's magnetosphere. However, not all front-side halo CMEs are geoeffective (*e.g.* Cane et al., 2000; Zhang et al., 2003; Yermolaev and Yermolaev, 2006; Gopalswamy et al., 2007). One explanation for the reported varying degrees of geoeffectiveness of halo CMEs is that not only full halo CMEs but also partial halos have been included in the analyses (Gopalswamy, 2009). Relations between several CME parameters and geomagnetic storms have been investigated: source location on the solar disk (Wang et al., 2002), initial projected speed (Srivastava and Venkatakrishnan, 2004) or radial velocity (Michalek et al., 2007) of the CME, magnetic field orientation of the CME source region (Kang et al., 2006), and various parameters related to the direction of the CME (Michalek et al., 2007; Kim et al., 2008; Shen et al., 2014; Lee et al., 2014). Based on only solar observations, long-term (order of days) forecast models of geomagnetic storms with varying success rates and reliability have been created (see *e.g.* Kim et al., 2010; Dumbović et al., 2015; Shanmugaraju et al., 2015, and references therein). On the other hand, short-term forecasts can be performed by measuring solar wind parameters and magnetic fields at Lagrange L1 point 1.5 million kilometres from the Earth towards the Sun (Temerin and Li, 2002, 2006; Pallocchia et al., 2006; Saiz et al., 2008; Ji et al., 2012; Rathore et al., 2015, Podladchikova et al., 2018, and references therein). Although significantly more reliable than long-term forecasts, the short-term forecasts suffer from the very short ($\lesssim 1$ h) warning time.

Coronal mass ejections are often associated with solar energetic particle (SEP) events (Gopalswamy et al., 2008; Park et al., 2012). Gleisner and Watermann (2006a,b) proposed to use the flux of $\geqslant 10$ MeV protons as an indicator of an approaching potentially geoeffective CMEs to reduce false alarms. Recently Le et al. (2016) suggested that SEP intensity-time profiles can be classified in three types with the CMEs associated with each type having different geoeffectiveness. The SEP intensity-time profiles were related to

dynamic behaviour of the ICMEs and propagation of the shocks driven by these ICMEs and thereby to their geoeffectiveness.

While SEPs are accelerated at or close to the Sun and usually observed soon ($\lesssim$ few hours) after the launch of the CME, the energetic storm particle (ESP) events are increases of particle intensities associated with the passing of an interplanetary shock with the observer (Cohen, 2006; Mäkelä et al., 2011). Since ESPs are associated with interplanetary shocks and thus can be used as a warning of a disturbance approaching the Earth, it has been proposed that ESPs could be used for mid-term (hours to a day) forecasting of geomagnetic storms or as an additional source of information for improving the reliability of the forecasts based only on remote solar observations (Smith et al., 2004; Valtonen et al., 2005; Smith and Murtagh, 2009; Lam, 2009). Using both SEP and ESP observations Valtonen et al. (2005) demonstrated the feasibility of such observations in evaluating geoeffectiveness of full and partial halo CMEs. The method was based on the time difference between the SEP event onset and the related ESP observation which also provided a proxy for the shock transit time from the Sun to the Earth.

The purpose of this article is to further investigate the possibilities and advantages of using energetic particle observations for mid-term geomagnetic storm forecasting. In Section 2 we present the data sources and describe the event selection and the procedure to associate the observed particle events and CMEs with geomagnetic storms. The data analysis of Section 3 starts with the presentation of the statistics and then proceeds to search for observational quantities suitable for mid-term forecasting of geomagnetic storms with a brief discussion of the lead time for storm forecasting provided by particle observations. The main results are summarised and discussed in Section 4 and conclusions are presented in Section 5.

2. Data sources and event selection

The starting point of this investigation was SEP–ESP events, *i.e.* particle events consisting of both a solar energetic particle event and an associated energetic storm particle event. SEPs related to CMEs or flares are accelerated close to the Sun and can be identified at the vicinity of the Earth based on the velocity dispersion of particles at different energies. ESP events, on the other hand, are enhancements of particle intensities at a later time than the onset of the associated SEP event (observed at the spacecraft location), showing no velocity dispersion and having a maximum close to the passage of the shock and then decaying. For more details of SEP and ESP event indentification, see Valtonen et al. (2005).

This study covers the time period from May 1996 to December 2017. For searching SEP–ESP events, we used the proton measurements of the *Energetic and Relativistic Nuclei and Electron* experiment (ERNE) (Torsti et al., 1995) aboard the *Solar and Heliospheric Observatory*

(SOHO) (Domingo et al., 1995) at two energies, 2 MeV (1.78–2.16 MeV) and 20 MeV (16.9–26 MeV). These two proton energies were selected because they are at the lower ends of the operational energy ranges of the two sensors of ERNE and thus provide the highest statistics. ERNE data are available at https://srl.utu.fi/erne_data/. In some cases, in particular for covering major data gaps of ERNE or in occurrences of ERNE saturation, we also used proton data from the *Geostationary Operational Environmental Satellites* (GOES) (https://www.ngdc.noaa.gov/stp/satellite/goes/dataaccess.html). Occurrence times of interplanetary shocks related to the observed ESP events were obtained from the online catalog of SOHO/CELIAS (http://umtof.umd.edu/pm/) or from the interplanetary shock database of the *Advanced Composition Observer* (ACE) and the *Wind* spacecraft (https://www.cfa.harvard.edu/shocks/). Both SOHO and ACE spacecraft operate in a halo orbit around the Lagrange L1 point of the Sun–Earth system. In its initial mission phase Wind had an orbit bringing it occasionally inside the magnetosphere. In early 2004 it was also permanently placed in a halo orbit around L1. GOES satellites are operating in geostationary orbits.

The CME catalog of the SOHO *Large Angle Spectroscopic Coronagraph* (LASCO) (Brueckner et al., 1995) at https://cdaw.gsfc.nasa.gov/CME_list/ was used to select the CMEs associated with the SEP events. In general, SEP events were associated with fast (>400 km s^{-1}) and wide (>60°) CMEs closest in time to the onsets of the SEP events at 20 MeV. In most cases it was also possible to use previous publications (e.g. Cane et al., 2010; Paassilta et al., 2017) as support for associating CMEs with SEP events. We assume the CME launch sites to coincide with those of the associated solar flares for which we used the locations given at https://hesperia.gsfc.nasa.gov/goes/goes_event_listings/ for the GOES soft X-ray flares.

The geomagnetic equatorial Dst index (disturbance storm-time index) is used for classifying geomagnetic storms. We use a simplified classification of Loewe and Prölss (1997) dividing geomagnetic storm into moderate storms with -100 nT $<$ Dst $\leqslant -50$ nT and strong storms with Dst $\leqslant -100$ nT. Henceforth Dst represents the minimum value of the index during a storm period. CMEs are considered geoeffective if they are followed by a geomagnetic storm with Dst $\leqslant -50$ nT (Gopalswamy et al., 2007; Ameri and Valtonen, 2017). Hourly Dst values were obtained from the World Data Center for Geomagnetism, Kyoto http://wdc.kugi.kyoto-u.ac.jp/dstdir/. For most events of this investigation the final Dst values were available, but for two events in 2015 we used the provisional values and for two evens in 2017 the quicklook Dst values.

For associating CMEs, and thus SEP and ESP events, with geomagnetic storms we used a similar technique as Ameri and Valtonen (2017). The drag-based model of Vršnak et al. (2013) was used to estimate the arrival time at 1 AU of an ICME corresponding to an observed CME. If a geomagnetic storm with minimum Dst $\leqslant -50$ nT was found within a ± 24 h time window from the predicted arrival time of the ICME, the related CME was associated with the storm. If a storm occurred within the arrival time windows of several ICMEs, the CME with the arrival time closest to the Dst minimum was taken as the cause of the storm. If also several storms were observed within the arrival time windows, the CME–storm pairs were selected according to their temporal sequence. For more details of the method of associating storms with CMEs see Ameri and Valtonen (2017) or Kim et al. (2005) and Shanmugaraju et al. (2015) who used similar techniques. We also used existing catalogs and previous publications, such as Zhang et al. (2007a) and Richardson and Cane (2010) (http://www.srl.caltech.edu/ACE/ASC/DATA/level3/icmetable2.htm) to assist associating CMEs with geomagnetic storms. In the process of associating CMEs with geomagnetic storms we also investigated other possible sources, such as high-speed solar wind streams, and discarded such events from the analysis.

3. Data analysis

3.1. Statistics

When searching ERNE proton data through the time period 1996–2017 we found altogether 65 SEP–ESP events, for which we were able to determine the SEP event onset time and the ESP peak time and to associate the events with CMEs and geomagnetic storms with Dst $\leqslant -50$ nT. Sixty events were identified at 2 MeV and 51 at 20 MeV. In most cases, when ESPs were observed at 2 MeV they were also observed at 20 MeV. One could expect that when ESPs are observed at 20 MeV they would be visible also at 2 MeV. However, during four events the low-energy detector of ERNE had data gaps, and in one event it was not possible to determine the onset time of the SEP event at 2 MeV due to high background caused by a preceding SEP event. On the other hand, not in all 65 SEP–ESP events the flux of ESP protons was high enough to be observed at the relatively high energy of 20 MeV. Therefore, to reach the best efficiency it is useful to apply two widely different energies for identifying the events.

Twenty-four of the 65 SEP–ESP events were associated with moderate storms (-100 nT $<$ Dst $\leqslant -50$ nT) and 41 with strong storms (Dst $\leqslant -100$ nT). Fourteen of the strong storms had Dst $\leqslant -200$ nT.

The 65 SEP–ESP events associated with geomagnetic storms are listed in Table A.3 in the Appendix A. A typical set of observations demonstrating the time sequence of events is presented in Fig. 1. The plot shows proton intensities at 2, 20, an 56 MeV as function of time for the event of August 4, 2011 together with the CME launch time, its predicted arrival at 1 AU, the observed shock time, the start time of the associated ICME, and the time dependence of the Dst index.

In addition to the 65 well-identified events, we recorded 19 uncertain SEP–ESP events and 10 ESP events associated
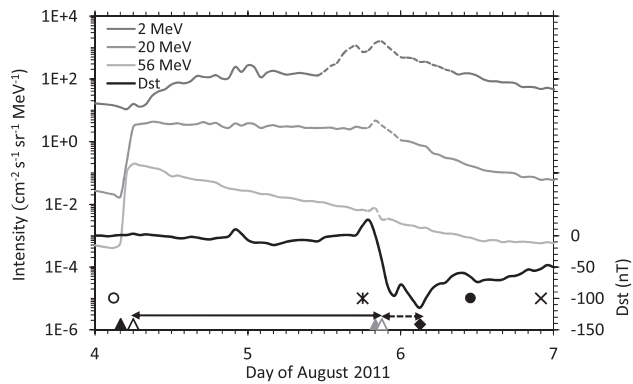
Fig. 1. Proton intensities (left vertical scale) and the Dst index (right vertical scale) as function of time during the SEP–ESP event of August 4, 2011 and the subsequent geomagnetic storm. The nominal proton energies from top to bottom are 2, 20, and 56 MeV. The dashed parts of the curves indicate the times of appearance of ESPs. The open circle is the launch time of the CME from the Sun and the filled circle its predicted arrival time at 1 AU. The asterix is the observed time of the interplanetary shock, and the x symbol is the observed start time of the ICME. The open and filled black triangles are the SEP onset times at 2 MeV and 20 MeV, respectively. The open and filled grey triangles are the corresponding ESP peak times. The black diamond indicates the Dst minimum time. The arrow-headed black line shows the time difference between ESP peak time and SEP onset time at 2 MeV and the arrow-headed dashed line demonstrates the time difference between the minimum Dst and the ESP peak time.

with geomagnetic storms (9 moderate and 1 strong storm) but without an SEP counterpart. The difficulties in reliable identification of SEP–ESP events, in particular the time of the ESP peak intensities, were related to large fluctuations of particle intensities at the time of the expected ESP events, and in some cases were related to the uncertainty of associating an ESP event with an SEP event. The uncertain events and the events with only ESPs observed were not included in the analysis presented in Section 3.2.

From the study period we further found 30 SEP–ESP events (24 observed at 2 MeV and 15 at 20 MeV) which were associated with CMEs, but not associated with geomagnetic storms or were associated with geomagnetic activity with Dst > -50 nT. Thus, from the study period we identified altogether 95 SEP–ESP events with 68% of these associated with geomagnetic storms. To complete the statistics of particle events, we identified 45 SEP events at 20 MeV without ESP counterparts but associated with geomagnetic storms caused by CMEs. Thirty-three of these were associated with moderate and 12 with strong storms. Finally, there were 139 SEP events observed at 20 MeV not associated with geomagnetic storms.

From the records of the Kyoto world data centre for geomagnetism we found 297 geomagnetic storms during the study period with Dst $\leqslant -50$ nT which we were able to associate with CMEs. Of these 201 were moderate and 96 strong storms. Of the strong storms all except two were caused by disturbances consisting of both an interplanetary (IP) shock and an ICME. The two exceptions were associated with only an IP shock. Roughly half, 122 moderate

and 36 strong storms of the total 297, were not associated with either SEP or ESP events at 20 MeV. The statistics of the particle events and geomagnetic storms together with the average minimum Dst values and standard errors (errors of the mean) and the causes of the storms are summarised in Table 1. Table 1 also shows the percentages of true hits, missed storms, and false alarms when using SEP–ESP events for forecasting all geomagnetic storms and separately for moderate and strong storms. These results will be discussed in Section 4.

The percentage of geomagnetic storms in four ranges of Dst with and without SEP–ESP associations are presented in Fig. 2. Only a small portion (12%) of the moderate storms are associated with SEP–ESP events, but the portion increases with the storm strength reaching 77% in the Dst range $[-200, -300]$ nT. For the strongest storms (Dst < -300 nT) the portion of uncertain SEP–ESP events is significant. This reflects the strongly disturbed conditions in interplanetary space preceding very strong geomagnetic storms.

3.2. Correlation analysis

We investigated the dependence of the logarithm of the absolute value of the minimum Dst on various parameters describing the characteristics of the particle events and coronal mass ejections. We used the logarithm of Dst because in our data set this quantity is more closely normally distributed than the observed Dst values themselves.

Fig. 3 a and b show the scatter plots of $\log_{10}|\text{Dst (nT)}|$ as function of the time difference between the SEP onset and ESP peak times, $\Delta t_{ESP-SEP}$, at energies 2 MeV and 20 MeV, respectively. The plots also show the linear regression lines with the corresponding equations and their 98% confidence limits. The error bars of the time differences in Fig. 3 a and b mostly represent the uncertainties in determining the peak times (times of maximum intensity) of the energetic storm particles. We calculated the Pearson correlation coefficients and their uncertainties for the dependences between $\log_{10}|\text{Dst (nT)}|$ and $\Delta t_{ESP-SEP}$ by using the method of resampling with replacement. In this method, samples are randomly selected from the original data. The size of each sample is the same as the original one, but replacement means that the same data point can be selected in a sample more than once or left unselected. The random selection was repeated 10,000 times and for each sample the correlation coefficient was calculated. The reported correlation coefficient is the average of those 10,000 samples and the uncertainty is the standard deviation of the obtained distribution.

We also investigated the effect of uncertainties in the time differences $\Delta t_{ESP-SEP}$ for the correlation coefficients. The uncertainties were considered as 1σ uncertainties. In this case, the correlation coefficients were calculated by randomly varying the data points according to a Gaussian distribution having the most probable value equal to the observed value and the standard deviation corresponding

Table 1
Particle events and geomagnetic storms 1996–2017.

| Events	Total	Mean and std. error of Dst (nT)	Moderate storms	Strong storms	IP shock & ICME	IP shock only	ICME only
Storm-associated							
SEP-ESP	65	-146 ± 10	24	41	63	2	0
Only ESP	10	-76 ± 6	9	1	6	3	1
Only SEP	45	-86 ± 5	33	12	37	5	3
Uncertain	19	-116 ± 25	13	6	7	12	0
No storm association							
SEP-ESP	30	–	–	–	–	–	–
Only SEP	139	–	–	–	–	–	–
Geomagnetic storms							
All	297	-100 ± 4	201	96	259	22	16
No particle event							
Association	158	-84 ± 3	122	36	141	6	11
Forecast statistics							
Hits (%)	22	–	12	43	–	–	–
Misses (%)	78	–	88	57	–	–	–
False alarms (%)	32	–	24	8	–	–	–
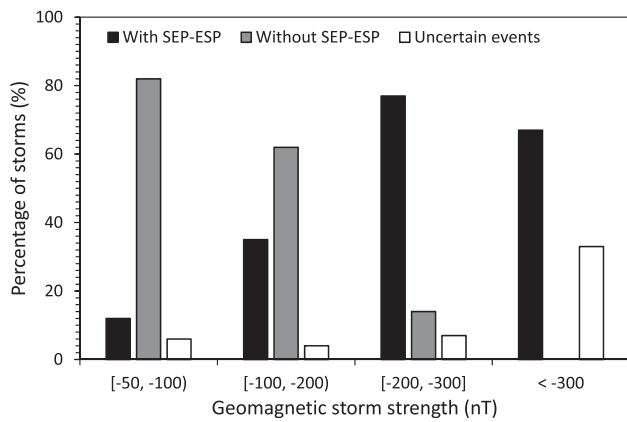
Fig. 2. Percentages of geomagnetic storms in four strength ranges with and without SEP–ESP associations. Uncertain events are those for which it was not possible to determine a reliable ESP peak time or association between SEP and ESP.

to the uncertainty of each point. Again, the correlation coefficient was calculated for each sample and the average value and the standard deviation of the distribution obtained when repeating this procedure 10,000 times represents the estimated correlation coefficient and its uncertainty. Since the uncertainties in $\Delta t_{ESP-SEP}$ are asymmetric, we used separate Gaussian distributions for positive and negative deviations from the most probable values with the rate of occurrence of positive and negative values weighted according to the relative magnitudes of the positive and negative uncertainties. Furthermore, in the analysis each point was weighted with the inverse square of the corresponding total uncertainty. This method and the method of resampling with replacement produced the same correlation coefficients within error limits, but the uncertainties given by the resampling method were slightly larger. Therefore, all correlation coefficients and their
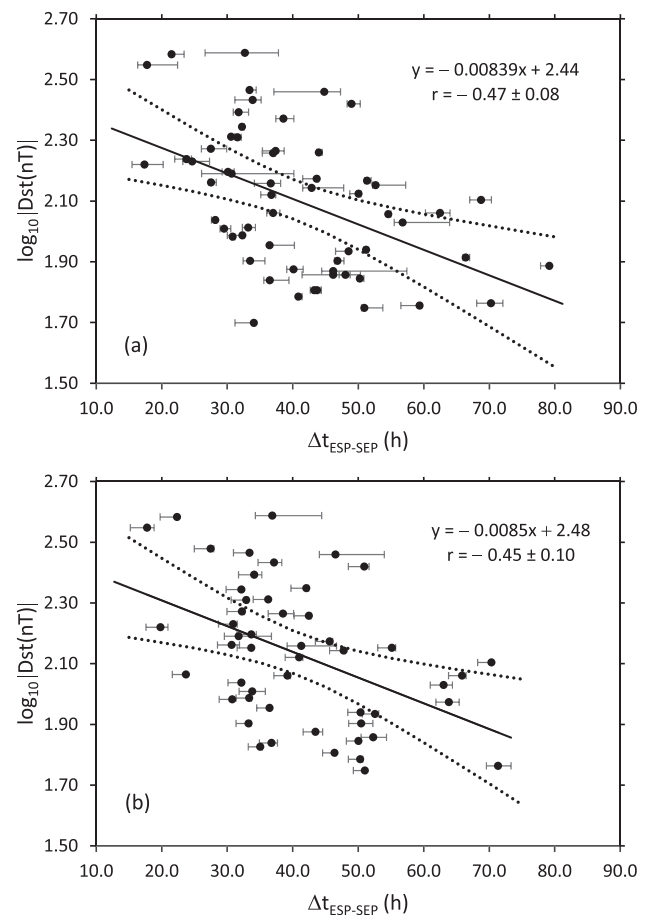

Fig. 3. Scatter plot of the logarithm of the absolute values of the minimum Dst as function of the time difference between the ESP peak time and SEP onset times at 2 MeV (a) and 20 MeV (b). The best-fit linear regression lines are shown by the black lines and the dotted lines are the 98% confidence limits. The regression equations and the calculated correlation coefficients with their standard deviations are shown in the plots.

uncertainties derived in this investigation are based on the resampling method.

The most significant correlations between the logarithm of the absolute value of the minimum Dst index and various parameters or combinations of parameters are summarised in Table 2. We found the correlation coefficients between $\log_{10}|\text{Dst (nT)}|$ and $\Delta t_{ESP-SEP}$ to be $r = -0.47 \pm 0.08$ and $r = -0.45 \pm 0.10$ at 2 MeV and 20 MeV, respectively. The linear fits are shown in Fig. 3. Although there is quite significant scatter, it is evident that there is a relation between the difference of the ESP peak time and the SEP onset time and the strength of the geomagnetic storm: the shorter the time difference, which also approximates the ICME/shock transit time from the Sun to the Earth, the stronger the storm. Equal correlation was found between the CME direction parameter (DP) and the logarithm of Dst. We define and determine the direction parameter following Moon et al. (2005) (see also Kim et al., 2008; Moon et al., 2009). The direction parameter quantifies the symmetric characteristics of a CME seen in a coronagraph image. The data for $\log_{10}|\text{Dst (nT)}|$ *v.s.* DP are presented in Fig. 4. For DP, there is no difference between the 2 and 20 MeV events. Another parameter related to energetic storm particles is their observed maximum energy. The correlation coefficient between the logarithm of the ESP maximum energy and the logarithm of the Dst index was $r = 0.44 \pm 0.11$. Correlation is expected, because ESP maximum energy reflects the strength of the shock accelerating the particles with the tendency of stronger shocks causing stronger geomagnetic storms. Weaker correlations were found for the maximum energy of solar energetic particles and the angular distance (in rad) of the source region (flare) from the solar disk centre (Table 2).

It is noteworthy that in our dataset there was no correlation between the CME initial speed and $\log_{10}|\text{Dst (nT)}|$
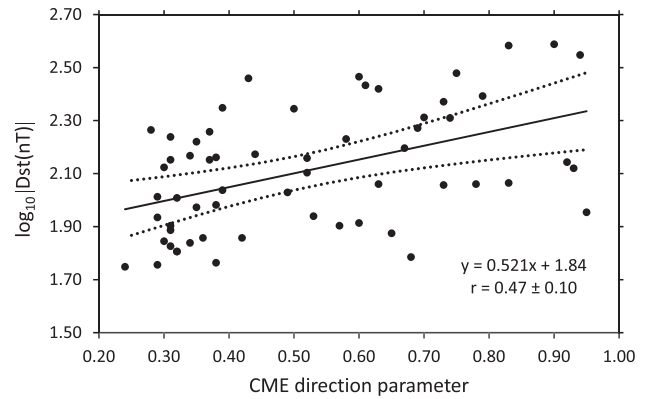

Fig. 4. Scatter plot of the logarithm of the absolute values of the minimum Dst as function of the CME direction parameter. The linear regression line is shown by the black line and the dotted lines are the 98% confidence limits. The regression equation and the calculated correlation coefficient with its standard deviation are shown in the plot.

($r = 0.07 \pm 0.13$). As well, the flare flux or the flare longitude did not significantly correlate with the storm strength. Furthermore, there was no correlation between the storm strength and the peak intensity of ESPs. It might be expected that the ESP peak intensity also depends on the shock strength, but it has been shown that there is no simple relation between the shock parameters and ESP maximum intensity (*e.g.* Lario et al., 2005). There was a weak correlation between the storm strength and the maximum SEP energy (Table 2), which probably indicates stronger shocks near the Sun with increasing maximum SEP energies.

In addition to single independent variable correlations we also investigated correlations between $\log_{10}|\text{Dst (nT)}|$ and various combinations of two or more independent variables. The combinations with the highest correlation

Table 2
Correlation coefficients between various parameters or combination of parameters and $\log_{10}|\text{Dst (nT)}|$ for SEP–ESP observations at 2 and 20 MeV.

One independent variable					
Energy	Δt	DP	$\log_{10}(E_{ESP}^{max})$	$\log_{10}(E_{SEP}^{max})$	α
2 MeV	-0.47 ± 0.08	0.47 ± 0.10	0.44 ± 0.11	0.33 ± 0.16	-0.32 ± 0.11
20 MeV	-0.45 ± 0.10	0.47 ± 0.10	0.44 ± 0.11	0.33 ± 0.16	-0.32 ± 0.11
Two independent variables					
Energy	Δt, DP	Δt, $\log_{10}(E_{ESP}^{max})$	Δt, $\log_{10}(E_{SEP}^{max})$	Δt, v_{CME}	Δt, α
2 MeV	0.64 ± 0.08	0.56 ± 0.07	0.51 ± 0.10	0.51 ± 0.08	0.53 ± 0.09
20 MeV	0.59 ± 0.10	0.43 ± 0.09	0.57 ± 0.12	0.48 ± 0.09	0.55 ± 0.10
Energy	$\log_{10}(E_{ESP}^{max})$, $\log_{10}(E_{SEP}^{max})$	DP, $\log_{10}(E_{ESP}^{max})$	DP, $\log_{10}(E_{SEP}^{max})$	DP, v_{CME}	DP, α
2, 20 MeV	0.44 ± 0.14	0.61 ± 0.08	0.52 ± 0.11	0.52 ± 0.10	0.48 ± 0.10
Three independent variables					
Energy	Δt, v_{CME}, $\log_{10}(E_{ESP}^{max})$	Δt, DP, $\log_{10}(E_{ESP}^{max})$	Δt, DP, $\log_{10}(E_{SEP}^{max})$	Δt, DP, v_{CME}	DP, v_{CME}, $\log_{10}(E_{ESP}^{max})$
2, 20 MeV	0.62 ± 0.06	0.68 ± 0.07	0.61 ± 0.09	0.67 ± 0.08	0.62 ± 0.08

$\Delta t \equiv \Delta t_{ESP-SEP}$ = time difference between ESP peak time and SEP onset time.
DP = CME direction parameter.
E_{ESP}^{max} = ESP maximum energy (MeV).
E_{SEP}^{max} = SEP maximum energy (MeV).
α = angular distance of flare location from disk centre (rad).
v_{CME} = CME initial speed.

coefficients are presented in Table 2. It is clear that the best two-variable combination explaining the storm strength is $\Delta t_{ESP-SEP}$ combined with DP. In Fig. 5 a we present $\log_{10}|$ Dst (nT)$|$ calculated from these two variables as function of the observed one. The calculated values are based on the multiple linear regression equation shown in the plot. Adding $\log_{10}[E^{max}_{ESP}(MeV)]$ or v_{CME} in this combination slightly improves the correlation coefficient (Table 2 and Fig. 5 b). Multiple linear regression shows that $\Delta t_{ESP-SEP}$ and DP are the most significant explaining variables also in these three-variable combinations. Performing stepwise regression with all available variables also shows that $\Delta t_{ESP-SEP}$ and DP are the only explaining variables at significance level $> 98\%$. Nevertheless, as indicated by the correlation coefficient, Fig. 5 b shows a slightly better dependence between the calculated and observed $\log_{10}|$ Dst (nT)$|$ compared to Fig. 5 a. When using the three independent variable combination, the absolute difference and the standard error between the observed and calculated

Dst is 46 ± 6 nT for the 2 MeV events. A closely similar result (48 ± 7 nT) was obtained fro the 20 MeV events.

3.3. ESP lead time for forecasting

An expected advantage of using solar energetic particle and energetic storm particle observations in geomagnetic storm forecasting is that such observations provide longer lead time before storm occurrence than solar wind measurements. In Fig. 6 a we present the distributions of ESP lead times, *i.e.* the differences between the time of Dst minimum and the peak time of ESPs at 2 and 20 MeV. The bin width in Fig. 6 a is 4 h. At both energies the distributions are broad with a maximum at 8 h followed by a tail extending in a few cases over 24 h. The approximate average lead time and its standard deviation is (15 ± 10) hours. We note that even a longer lead time could be achieved by using the ESP onset times instead of the peak times. In our dataset the ESP onset time was on average 3 h before the peak time. In real-time observations an accurate identification of the peak time may be difficult, and an earlier warning when using the onset time would also be an advantage. Furthermore, a real-time monitoring of the rise of the intensity would permit an
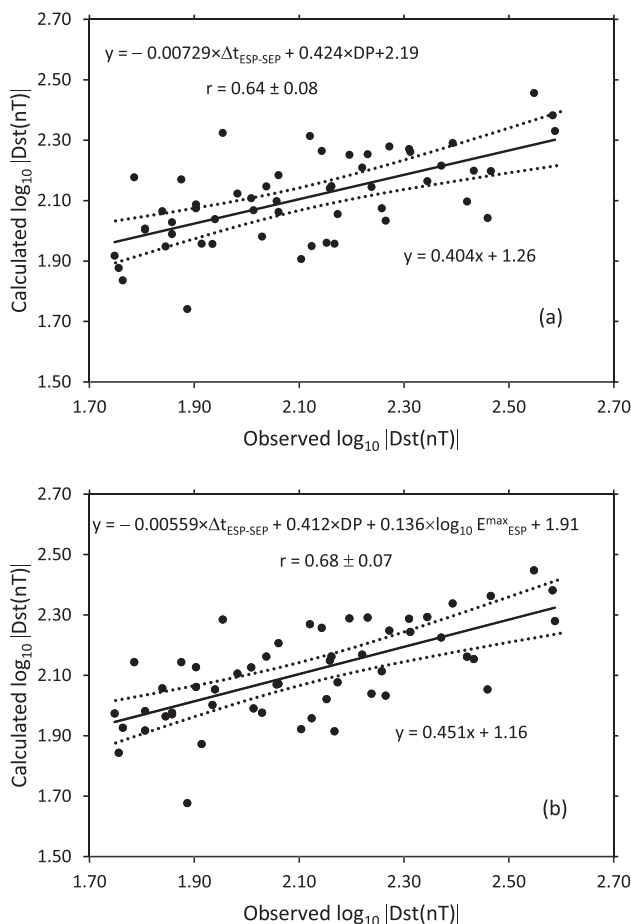

Fig. 5. (a) Calculated $\log_{10}|$Dst (nT)$|$ as function of the observed one based on two independent variable ($\Delta t_{ESP-SEP}$ and DP) regression. The regression equation, the calculated correlation coefficient and its standard deviation are shown at the top of the plot. The black line is a linear fit line to the data points according to the equation shown in the lower part of the plot and the dotted lines are the 98% confidence limits of the regression line. (b) As (a), but for three independent variable ($\Delta t_{ESP-SEP}$, DP, and $\log_{10}[E^{max}_{ESP}(MeV)]$) regression.
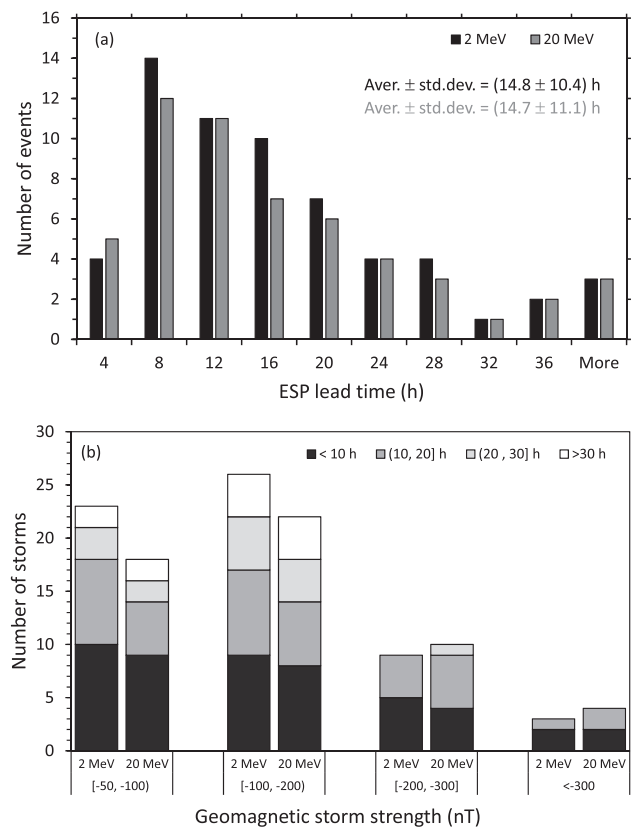

Fig. 6. (a) Distributions of the differences between the time of minimum Dst and the peak time of ESPs observed at 2 MeV (black columns) and 20 MeV (grey columns). The averages and the standard deviations of the distributions are given in the plot. (b) Number of storms with different lead times obtained at 2 MeV and 20 MeV proton energies in four ranges of the storm strength.

automatic alarm when exceeding a preset (relative) threshold after the onset and would then provide a possibility to verify the true onset time.

Fig. 6 b shows the number of storms with different lead times in four ranges of the storm strength. It is apparent that when using the ESP peak times, the longest lead times can only be achieved for moderate storms and for storms in the Dst range $[-100, -200]$ nT. Although the average lead time for all strong storms was still (14 ± 10) hours, the shortest lead time was only 2 h. For storms with Dst < -200 nT the average lead time was (9.3 ± 5.5) hours.

We also investigated the distributions of the differences between the ESP peak time and the shock and ICME arrival times, and the time of occurrence of the minimum southward IP magnetic field component. The difference between the shock arrival time and the ESP peak time had a large maximum at 0.0 ± 0.5 hours with roughly symmetric low wings extending on both sides up to 3 h. The distribution of the differences between the ICME arrival time and the ESP peak time was rather flat from 2 to 24 h with some outliers at larger differences. For the minimum southward magnetic filed component the distribution extended from 0 to 24 h also with some outliers at later times. The distribution was asymmetric with a clear maximum at 4 h and an average of 7.5 h.

4. Summary of main results and discussion

We have investigated relations between the occurrence and characteristics of energetic particle events in interplanetary space and geomagnetic storms with Dst $\leqslant -50$ nT during the period 1996–2017 with the aim to use such relations for improving mid-term forecasts of geomagnetic storms. Following Valtonen et al. (2005) we focused on proton events consisting of two components: SEPs accelerated near the Sun and ESPs observed at the time of the shock passing the spacecraft. During the study period we identified altogether 95 SEP–ESP events at 2 MeV or 20 MeV proton energies for which it was possible to determine the SEP onset time, ESP peak time, and CME association. We then searched for geomagnetic storms with Dst $\leqslant -50$ nT caused by CMEs. We assumed that those SEP–ESP events for which the SEP parts were associated with the storm-causing CMEs were also associated with the geomagnetic storms. We found that 65 out of the 95 (68%) SEP–ESP events were associated with a geomagnetic storm, while for 30 events we did not manage to find association with geomagnetic storms or the associated geomagnetic activity was low with Dst > -50 nT. Twenty-four of the 65 SEP–ESP events were associated with moderate storms (-100 nT $< $ Dst $\leqslant -50$ nT) and 41 with strong storms (Dst $\leqslant -100$ nT).

In addition to the SEP–ESP events associated with geomagnetic storms, we found 45 events consisting of only SEPs and 10 events of only ESPs which we were able to associate with geomagnetic storms caused by CMEs (Table 1). There were also 19 uncertain events during the study period for which either the ESP peak time or the SEP–ESP association could not be reliably determined. Furthermore, at 20 MeV we identified 139 SEP events which were not associated with geomagnetic storms. The average minimum Dst of geomagnetic storms associated with SEP–ESP events was (-146 ± 10) nT. For events with only SEPs and for events with only ESPs the average minimum Dst was (-86 ± 5) nT and (-76 ± 6) nT, respectively. The difference in the average minimum Dst between the group of SEP–ESP events and the other two groups is significant. Le et al. (2016) studied the geoeffectiveness of CMEs associated with large proton events during solar cycle 23. They classified the events according to their intensity-time profiles to events with only one peak and events with two peaks or continuously rising intensities until the CME-driven shock reaches the Earth. These correspond to our events with only SEPs, and SEP–ESP or only ESP events. Le et al. (2016) found that most of the CMEs associated with only SEP events were not geoeffective. Most of the CMEs associated with events with two peaks, and in particular events with the intensity in the second peak (ESP) higher than in the first peak (SEP), were able to produce intense (-200 nT $\leqslant$ Dst < -100 nT) or great storms (Dst $\leqslant -200$ nT).

While the portion of all geomagnetic storms caused by CMEs, which are associated with SEP–ESP events (hits in Table 1) is low (22%), it is significantly higher (43%) for strong storms. Furthermore, almost all storms with Dst $\leqslant -200$ nT (14/19 or 74%) were associated with SEP–ESP events. Only one was not associated with energetic particles at all and one with an SEP event only. The rest three were in our category of uncertain events, which reflects the very disturbed conditions in interplanetary space preceding very strong geomagnetic storms. Nevertheless, statistically 57% of the strong storms (Dst $\leqslant -100$ nT) caused by CMEs could not be forecast based on SEP–ESP observations alone. False alarms would have been caused in 32% of all the storms and only in 8% of the strong storms. The relative amounts of false alarms in moderate and strong storms given in Table 1 are based on the predictions given by the equation shown in Fig. 5 b for the SEP–ESP events not associated with geomagnetic storms.

Comparison of characteristics of CMEs and other solar phenomena leading to geomagnetic storms but lacking energetic particles to those with also energetic particle associations showed that in the former group the average CME speed $((580 \pm 30)$ kms$^{-1})$ and flare flux $(((3 \pm 1) \times 10^{-5}$ Wm$^{-2}))$ were lower, the average source location was far from the magnetically well connected region $(-9° \pm 4°)$, and the events were poorly associated with decametric-hectometric type II radio bursts (21%) with only short durations $((1.5 \pm 0.6$ h)$)$ compared to the latter group $((1310 \pm 60)$ kms^{-1}, $((7 \pm 3) \times 10^{-5}$ Wm$^{-2})$, $17° \pm 4°$, 83%, and $(16 \pm 2$ h)$)$. Thus, solar events of the first group tend to be too weak to be efficient particle accelerators or in some cases originate from solar regions from which energetic particles do not easily reach the Earth.

Energetic particles mostly appear with CMEs originating from the western hemisphere being well associated with long-duration type II radio bursts. Vasanth et al. (2015) has shown that for such CMEs, with low end-frequency of type II bursts, the possibility of having geomagnetic storms increases in general. On the other hand, the differentiating factors between CMEs not causing storms, but associated with energetic particles, and those leading to storms were the CME direction parameter and the angular distance of the source region from the disk centre. The average DP for storm-causing CMEs associated with SEP–ESP events was 0.52 ± 0.03, while for those not causing storms, but still associated with energetic particles, it was 0.40 ± 0.02. The corresponding average values for the angular distance from the disk centre were 0.66 ± 0.06 and 0.86 ± 0.08, respectively. Although a CME is directed away from the Earth, and therefore not causing a storm, ESPs can still be observed near the Earth due to the wider extent of the shock.

For the 65 storm-associated SEP–ESP events we studied correlations between several parameters characterising the particle events or the associated solar phenomena and the minimum value of the Dst index during the storms. As Table 2 shows, there are no significant differences in the correlations at 2 and 20 MeV. Therefore, observation at either 2 or 20 MeV can be used. Although in general ESPs at 2 MeV are more frequently observed, in some cases ESP peak times and in particular SEP onset times can be more reliably determined at 20 MeV. We found a relatively good correlation ($r = -0.47 \pm 0.08$) for the difference between the ESP peak time and SEP onset time with the logarithm of the absolute value of the minimum Dst. Equally good correlation ($r = 0.47 \pm 0.10$) was found for the CME direction parameter. Somewhat better correlation was reported between the ESP onset time–SEP onset time difference and Dst by Valtonen et al. (2005) ($r = 0.69$). Also, Kim et al. (2010) and Shanmugaraju et al. (2015) have found somewhat better correlations between DP and Dst ($r = 0.60$ and $r = 0.57$, respectively). With an attempt to improve the correlation, we investigated combinations of various parameters. The best correlation for two independent variables was obtained for the combination of $\Delta t_{ESP-SEP}$ and DP. The correlation coefficient achieved was $r = 0.64 \pm 0.08$ at 2 MeV. Adding a third independent variable, the logarithm of the maximum energy of ESPs, still slightly improved the correlation. We suggest that the formula $\log_{10}|\text{Dst (nT)}| = -0.00559 \times \Delta t_{ESP-SEP}(h) + 0.412 \times DP + 0.136 \times \log_{10}[E_{ESP}^{max}(\text{MeV})] + 1.91$ best reproduces the observed $\log_{10}|\text{Dst (nT)}|$ (Fig. 5) and can be used to estimate the ensued minimum Dst based on energetic particle and CME observations. As a verification for the formula, we calculated the predicted storm strengths for the storms associated with the SEP–ESP events. Of the moderate storms 57% were correctly predicted to be moderate storms. The corresponding percentage for strong storms was 87. Of the strong storms 13% were incorrectly predicted to be moderate

storms, and of the moderate storms 43% were incorrectly predicted to be strong storms.

Kim et al. (2010) investigated the dependence of geomagnetic storm strength on CME parameters during the time period of 1997–2003. They separated the events in two groups depending on the magnetic field orientation of the source region. Kim et al. (2010) proposed storm prediction formulae, which for the southward magnetic field orientation included the CME direction parameter and the CME speed as independent variables, and for the northward events the CME source locations as the third independent variable. For their southward and northward models they found correlation coefficients of 0.66 and 0.80, respectively. A similar model as Kim et al. (2010) was suggested by Shanmugaraju et al. (2015) for events during the rising phase of solar cycle 24. Shanmugaraju et al. (2015) also concluded the prediction models are solar cycle dependent. Our study covered a time period of almost two solar cycles. Possible dependences on solar cycles or solar cycle phases were not taken into account.

We investigated the lead time (warning time) provided by SEP–ESP observations for storm forecasting. We define the lead time as the difference between the Dst minimum time and the ESP peak time. From the distribution of the differences between the time of minimum Dst and the peak time of ESPs (Fig. 6) we found the most probable lead time of 8 h with the average of (15 ± 10) hours, approximately the same at 2 and 20 MeV. This is similar to the lead time from minutes to more than a day with the average of 7 h for large storms reported by Smith and Murtagh, 2009 by using lower energy ions.

It is well known that the single parameter best explaining the strength of a geomagnetic storm is the southward component of the IP magnetic field (B_s). In-situ measurements of IP magnetic field can, however, provide only a short warning time of $\lesssim 1$ h (e.g. Saiz et al., 2008) (see also Kim et al., 2014, and references therein). We inspected the occurrence times of ESP peaks compared to the time of minimum B_s in our dataset. We found the most probable ESP peak time (mode of the distribution) to be 4 h before the minimum B_s with the average of 7.5 h. The storm warning time by using ESPs could be increased by using the onset time of ESPs instead of the peak time. The ESP onset time could also be used to predict the shock arrival. For a limited number of events from 1996 to 2000 Valtonen et al. (2005) found an average lead time of 6 h for the ESP onset time compared to the shock arrival. For the current dataset the average ESP onset time was 3 h before the ESP peak time, while the peak time quite well coincided with the shock arrival time. When working with real-time observations, using the ESP onset time instead of the peak time would possibly provide a more robust time difference required for the suggested forecast formula and would also provide an earlier warning.

5. Conclusions

Based on correlations between the logarithm of the absolute value of the minimum Dst and various parameters characterising energetic particle events and coronal mass ejections, we have derived a simple equation, which can be used for mid-term forecasting of geomagnetic storm strengths. The three parameters used as input for calculating the storm strength are the difference between the ESP peak time and the onset time of the associated SEP event, the logarithm of the maximum ESP energy, and the CME direction parameter. Thus, only coronagraph observations of the CMEs and energetic particle measurements in interplanetary space are required for employing this technique. The correlation coefficient between the calculated and observed storm strength is 0.68 ± 0.07. The method provides an average warning time, *i.e.* the time from the observation of the maximum intensity of ESPs till the minimum of Dst, of (15 ± 10) hours.

Acknowledgements

Appendix A.

See Table A.3.

Table A.3
SEP–ESP events and associated CME direction parameters and values of the minimum Dst in 1996–2017.

N:o	Date	SEP onset time		ESP peak time		E_{ESP}^{max}	CME	Dst
	Year dd/mm	2 MeV hh:mm	20 MeV hh:mm	2 MeV dd/mm hh:mm	20 MeV dd/mm hh:mm	(MeV)	DP	(nT)
	1997							
1	07/04	18:37	15:17	10/04 13:01		4	0.60	−82
2	12/05	09:17	06:46	14/05 23:45	15/05 00:37	23	0.78	−115
	1998							
3	03/01	05:51		06/01 13:01		4	0.31	−77
4	02/05	20:02	14:18	04/05 02:37	04/05 02:34	36	0.70	−205
5	24/08	00:30[*]	23:15	26/08 07:10	26/08 07:00	63		−155
6	05/11	23:21	20:52	08/11 04:00	08/11 04:00	67	0.37	−142
	1999							
7	21/09	11:56	06:00	22/09 11:43		9	0.31	−173
	2000							
8	09/02	21:50		11/02 23:51	11/02 23:08	29	0.30	−133
9	04/04	18:33	16:15	06/04 15:21	06/04 14:47	36	0.43	−288
10	06/06	20:11	20:00	08/06 08:38	08/06 08:27	22	0.95	−90
11	14/07		10:57		15/07 14:24	387[**]	0.75	−301
12	10/08	01:15		11/08 15:49	11/08 15:45	45	0.73	−235
13	03/10	06:56		05/10 02:55		5		−182
14	10/10	12:45	6:27	12/10 21:31	12/10 21:29	20	0.49	−107
15	25/10	15:03	11:47	28/10 11:47	28/10 10:07	20	0.52	−127
16	08/11	23:40	23:40	10/11 06:30	10/11 06:25	33	0.38	−96
17	24/11	10:05	06:43	26/11 08:54	26/11 09:10	57	0.57	−80
	2001							
18	21/01	18:25	09:02	23/01 11:17	23/01 11:19	20	0.68	−61
19	25/03	14:05	14:54	27/03 17:17	27/03 17:15	33	0.53	−87
20	29/03	15:41	11:21	31/03 00:22	31/33 00:14	20	0.90	−387
21	02/04	03:57[*]	22:59	04/04 14:00		3		−50
22	10/04	10:30	06:54	11/04 20:22	11/04 20:02	20	0.61	−271
23	15/04	17:26	14:25	18/04 00:01		15	0.73	-114
24	24/09	14:31	11:31	25/09 20:01	25/09 21:20	63	0.32	−102
25	01/10	12:37	10:41	02/10 06:00	02/10 06:30	33	0.35	−166
26	19/10	08:40	02:50	20/10 12:09	20/10 11:04	31	0.69	−187
27	04/11	16:35	16:35	06/11 02:00	06/11 02:00		0.60	−292
28	22/11	21:45	21:45	24/11 06:00	24/11 05:55	387[**]	0.50	−221
29	26/12	07:21	06:05	29/12 05:36	29/12 05:25	66	0.38	−58

	2002							
30	17/04	12:19	10:17	19/04 07:57	19/04 07:55	45	0.44	−149
31	21/04	01:55	01:50	23/04 04:50	23/04 04:50	63	0.24	−57
32	22/05	06:47	02:31	23/05 10:57	23/05 10:40	62	0.39	−109
33	05/09	02:56[*]	20:33	07/09 15:55	07/09 15:01	72	0.37	−181
34	24/11	02:20[*]	22:43	26/11 21:37	26/11 21:05	20	0.32	−64
	2003							
35	18/03	16:29	13:37	20/03 12:11		7	0.32	−64
36	28/05	04:51	00:55	29/05 17:30	29/05 18:13	45	0.52	−144
37	28/10	12:35	12:30	29/10 06:20	29/10 06:15	63	0.94	−353
38	29/10	22:05	21:15	30/10 19:35	30/10 19:35	63	0.83	−383
39	02/11	18:00	17:40	04/11 06:30	04/11 06:25	33	0.34	−69
	2004							
40	25/07	23:07	16:23	26/07 23:45	26/07 23:17	105	0.58	−170
41	07/11	19:42	17:49	09/11 20:40	09/11 20:44	83	0.63	−263
	2005							
42	16/01	01:42	00:26	17/01 10:54		11	0.29	−103
43	20/01	09:19	07:33	21/01 17:37	21/01 16:53	33		−97
44	13/05	20:15	18:03	15/05 04:00	15/05 04:10	105	0.79	−247
45	14/07		13:00	16/07 00:14	16/07 00:02	57	0.31	−67
46	22/08	20:23	18:51	24/08 09:45	24/08 09:22	36	0.28	−184
47	13/09	23:35	23:20	15/09 09:05	15/09 08:35	33	0.31	−80
	2006							
48	13/12	07:47	04:09	14/12 13:53	14/12 13:50	90	0.67	−162
	2010							
49	01/08	19:35		03/08 17:45	03/08 18:40	30		−74
	2011							
50	04/08	08:03	05:23	05/08 21:03	05/08 20:34	57	0.63	−115
51	22/10	16:33		24/10 19:53		12	0.34	−147
	2012							
52	20.01	03:19	03:15	22/01 05:33	22/01 05:17	33	0.30	−70
53	24/02	12:00	12:00	26/02 23:21		11	0.29	−57
54	07/03	07:35	04:47	08/03 11:07	08/03 11:27	63	0.38	−145
55	14/06	21:03	16:57	16/06 21:34	16/06 21:30	57	0.29	−86
56	12/07	21:29	17:31	14/07 16:21	14/07 17:17	31	0.92	−139
	2013							
57	15/03	17:53	13:37	17/03 06:37	17/03 06:35	20	0.93	−132
58	29/09[**]	03:35[*]	01:25[*]	02/10 01:45		12	0.42	−72
	2014							
59	18/02		04:13		19/02 03:54	29	0.83	−116
60	25/02		03:00		27/02 18:50	57	0.35	−94
61	10/09	23:45	20:13	12/09 15:51	12/09 15:41	23	0.65	−75
	2015							
62	15/03		05:00		16/03 23:05	36	0.39	−222
63	21/06	10:47	09:27	22/06 18:21	22/06 18:21	62	0.74	−204
	2017							
64	14/07	06:11	03:07	16/07 06:13	16/07 07:25	20	0.36	−72
65	06/09		13:25	08/09 00:03	07/09 23:05	36	0.31	−124

[*] Next day.
[**] From GOES.

References

Ameri, D., Valtonen, E., 2017. Investigation of the geoeffectiveness of disk-centre full-halo coronal mass ejections. Sol. Phys. 292, 79. https://doi.org/10.1007/s11207-017-1102-7.

Brueckner, G.E., Howard, R.A., Koomen, M.J., et al., 1995. The Large Angle Spectroscopic Coronagraph (LASCO). Sol. Phys. 162, 357–402. https://doi.org/10.1007/BF00733434.

Cane, H.V., Richardson, I.G., St. Cyr, O.C., 2000. Coronal mass ejections, interplanetary ejecta and geomagnetic storms. Geophys. Res. Lett. 27, 3591–3594. https://doi.org/10.1029/2000GL000111.

Cane, H.V., Richardson, I.G., von Rosenvinge, T.T., 2010. A study of solar energetic particle events of 1997–2006: their composition and associations. Geophys. Res. 115, A08101. https://doi.org/10.1029/2009JA014848.

Cohen, C.M.S., 2006. Observations of energetic storm particles: an overview. Washington DC Am. Geophys. Union Geophys. Monogr. Ser. 165, 275–282. https://doi.org/10.1029/165GM26.

Domingo, V., Fleck, B., Poland, A.I., 1995. The SOHO mission: an overview. Sol. Phys. 162, 1–37. https://doi.org/10.1007/BF00733425.

Dumbović, M., Devos, A., Vrnak, B., et al., 2015. Geoeffectiveness of coronal mass ejections in the SOHO era. Sol. Phys. 290, 579–612. https://doi.org/10.1007/s11207-014-0613-8.

Echer, E., Gonzalez, W.D., Tsurutani, B.T., Gonzalez, A.L.C., 2008. Interplanetary conditions causing intense geomagnetic storms (Dst ≤ -100 nT) during solar cycle 23 (1996-2006). J. Geophys. Res. (Space Phys.) 113, A05221. https://doi.org/10.1029/2007JA012744.

Echer, E., Tsurutani, B.T., Gonzalez, W.D., 2013. Interplanetary origins of moderate (-100 nT < Dst ≤ -50 nT) geomagnetic storms during solar cycle 23 (1996-2008). J. Geophys. Res. (Space Phys.) 118, 385–392. https://doi.org/10.1029/2012JA018086.

Gleisner, H., Watermann, J., 2006a. Concepts of medium-range (1 - 3 days) geomagnetic forecasting. Adv. Space Res. 37, 1116–1123. https://doi.org/10.1016/j.asr.2005.10.010.

Gleisner, H., Watermann, J., 2006b. Solar energetic particle flux enhancement as an indicator of halo coronal mass ejection geoeffectiveness. Space Weather 4, S06006. https://doi.org/10.1029/2006SW000220.

Gonzalez, W.D., Joselyn, J.A., Kamide, Y., et al., 1994. What is a geomagnetic storm? J. Geophys. Res. 99, 5771–5792. https://doi.org/10.1029/93JA02867.

Gonzalez, W.D., Tsurutani, B.T., Clúa de Gonzalez, A.L., 1999. Interplanetary origin of geomagnetic storms. Space Sci. Rev. 88, 529–562. https://doi.org/10.1023/A:1005160129098.

Gonzalez, W.D., Echer, E., Tsurutani, B.T., Clúa de Gonzalez, A.L., Dal Lago, A., 2011. Interplanetary origin of intense, superintense and extreme geomagnetic storms. Space Sci. Rev. 158, 69–89. https://doi.org/10.1007/s11214-010-9715-2.

Gopalswamy, N., Yashiro, S., Akiyama, S., 2007. Geoeffectiveness of halo coronal mass ejections. J. Geophys. Res. (Space Phys.) 112, A06112. https://doi.org/10.1029/2006JA012149.

Gopalswamy, N., Yashiro, S., Akiyama, S., et al., 2008. Coronal mass ejections, type II radio bursts, and solar energetic particle events in the SOHO era. Ann. Geophys. 26, 3033–3047. https://doi.org/10.5194/angeo-26-3033-2008.

Gopalswamy, N., 2009. Halo coronal mass ejections and geomagnetic storms. Earth Planets Space 61, 595–597. https://doi.org/10.1186/BF03352930.

Gosling, J.T., McComas, D.J., Phillips, J.L., Bame, S.J., 1991. Geomagnetic activity associated with earth passage of interplanetary shock disturbances and coronal mass ejections. J. Geophys. Res. 96, 7831–7839. https://doi.org/10.1029/91JA00316.

Ji, E.-Y., Moon, Y.-J., Gopalswamy, N., Lee, D.-H., 2012. Comparison of Dst forecast models for intense geomagnetic storms. J. Geophys. Res. (Space Phys.) 117, A03209. https://doi.org/10.1029/2011JA016872.

Kang, S.-M., Moon, Y.-J., Cho, K.-S., et al., 2006. Coronal mass ejection geoeffectiveness depending on field orientation and interplanetary coronal mass ejection classification. J. Geophys. Res. (Space Phys.) 111, A05102. https://doi.org/10.1029/2005JA011445.

Kim, R.-S., Cho, K.-S., Moon, Y.-J., et al., 2005. Forecast evaluation of the coronal mass ejection (CME) geoeffectiveness using halo CMEs from 1997 to 2003. Geophys. Res. 110, A11104. https://doi.org/10.1029/2005JA011218.

Kim, R.-S., Cho, K.-S., Kim, K.-H., et al., 2008. CME earthward direction as an important geoeffectiveness Indicator. Astrophys. J. 677, 1378–1384. https://doi.org/10.1086/528928.

Kim, R.-S., Cho, K.-S., Moon, Y.-J., et al., 2010. An empirical model for prediction of geomagnetic storms using initially observed CME parameters at the Sun. J. Geophys. Res. (Space Phys.) 115, A12108. https://doi.org/10.1029/2010JA015322.

Kim, R.-S., Moon, Y.-J., Gopalswamy, N., Park, Y.-D., Kim, Y.-H., 2014. Two-step forecast of geomagnetic storm using coronal mass ejection and solar wind condition. Space Weather 12, 246–256. https://doi.org/10.1002/2014SW001033.

Lam, H.-L., 2009. Enhancement of solar wind low-energy energetic particles as precursor of geomagnetic disturbance in operational geomagnetic forecast. Adv. Space Res. 43, 1299–1313. https://doi.org/10.1016/j.asr.2009.01.010.

Lario, D., Hu, Q., Ho, G.C., Decker, R.B., Roelof, E.C., Smith, C.W. 2005. Statistical Properties of Fast Forward Transient Interplanetary Shocks and Associated Energetic Particle Events: ACE Observations, Solar Wind 11/SOHO 16, Connecting Sun and Heliosphere 81-86. <http://adsabs.harvard.edu/abs/2005ESASP.592...81L>.

Le, G.-M., Li, C., Tang, Y.-H., et al., 2016. Geoeffectiveness of the coronal mass ejections associated with solar proton events. Res. Astron. Astrophys. 16, 14. https://doi.org/10.1088/1674-4527/16/1/014.

Lee, J.-O., Moon, Y.-J., Lee, K.-S., Kim, R.-S., 2014. Dependence of geomagnetic storms on their associated halo CME parameters. Sol. Phys. 289, 2233–2245. https://doi.org/10.1007/s11207-013-0466-6.

Loewe, C.A., Prölss, G.W., 1997. Classification and mean behavior of magnetic storms. J. Geophys. Res. 102, 14209–14214. https://doi.org/10.1029/96JA04020.

Mäkelä, P., Gopalswamy, N., Akiyama, S., Xie, H., Yashiro, S., 2011. Energetic storm particle events in coronal mass ejection-driven shocks. J. Geophys. Res. (Space Phys.) 116, A08101. https://doi.org/10.1029/2011JA016683.

Michalek, G., Gopalswamy, N., Yashiro, S., 2007. Prediction of space weather using an asymmetric cone model for halo CMEs. Sol. Phys. 246, 399–408. https://doi.org/10.1007/s11207-007-9081-8.

Moon, Y.-J., Cho, K.-S., Dryer, M., Kim, Y.-H., 2005. New geoeffective parameters of very fast halo coronal mass ejections. Astrophys. J. 624, 414–419 <http://adsabs.harvard.edu/abs/2005AGUSMSH23A..01M>.

Moon, Y.-J., Kim, R.-S., Cho, K.-S., 2009. Geometrical implication of the CME earthward direction parameter and its comparison with cone model parameters. Korean Astronom. Soc. 42, 27–32 <http://adsabs.harvard.edu/abs/2009JKAS...42...27M>.

Oliveira, D.M., Samsonov, A.A., 2018. Geoeffectiveness of interplanetary shocks controlled by impact angles: A review. Adv. Space Res. 61, 1–44. https://doi.org/10.1016/j.asr.2017.10.006.

Paassilta, M., Raukunen, O., Vainio, R., et al., 2017. Catalogue of 55-80 MeV solar proton events extending through solar cycles 23 and 24. J. Space Weather Space Clim. 7, A14. https://doi.org/10.1051/swsc/2017013.

Pallocchia, G., Amata, E., Consolini, G., Marcucci, M.F., Bertello, I., 2006. Geomagnetic D_{st} index forecast based on IMF data only. Ann. Geophys. 24, 989–999. https://doi.org/10.5194/angeo-24-989-2006.

Park, J., Moon, Y.-J., Gopalswamy, N., 2012. Dependence of solar proton events on their associated activities: Coronal mass ejection parameters. J. Geophys. Res. (Space Phys.) 117, A08108. https://doi.org/10.1029/2011JA017477.

Podladchikova, T., Petrukovich, A., Yermolaev, Y., 2018. Geomagnetic storm forecasting service StormFocus: 5 years online. J. Space Weather Space Clim. 8, A22. https://doi.org/10.1051/swsc/2018017.

Pulkkinen, T., 2007. Space weather: terrestrial perspective. Living Rev. Sol. Phys. 4, 1–60. https://doi.org/10.12942/lrsp-2007-1.

Rathore, B.S., Gupta, D.C., Kaushik, S.C., 2015. Effect of solar wind plasma parameters on space weather. Res. Astron. Astrophys. 15, 85–106. https://doi.org/10.1088/1674-4527/15/1/009.

Richardson, I.G., Cane, H.V., 2010. Near-earth interplanetary coronal mass ejections during solar cycle 23 (1996–2009). Sol. Phys. 264, 189–237. https://doi.org/10.1007/s11207-010-9568-6.

Richardson, I.G., Cane, H.V., 2012. Solar wind drivers of geomagnetic storms during more than four solar cycles. J. Space Weather Space Clim. 2, A01. https://doi.org/10.1051/swsc/2012001.

Saiz, E., Cid, C., Cerrato, Y., 2008. Forecasting intense geomagnetic activity using interplanetary magnetic field data. Ann. Geophys. 26, 3989–3998. https://doi.org/10.5194/angeo-26-3989-2008.

Schwenn, R., 2006. Space weather: The solar perspective. Living Rev. Sol. Phys. 3, 2–72. https://doi.org/10.12942/lrsp-2006-2.

Schwenn, R., dal Lago, A., Huttunen, E., Gonzalez, W.D., 2005. The association of coronal mass ejections with their effects near the Earth. Ann. Geophys. 23, 1033–1059. https://doi.org/10.5194/angeo-23-1033-2005.

Shanmugaraju, A., Syed Ibrahim, M., Moon, Y.-J., Mujiber Rahman, A., Umapathy, S., 2015. Empirical relationship between CME parameters and geo-effectiveness of halo CMEs in the rising phase of solar cycle 24 (2011–2013). Sol. Phys. 290, 1417–1427, https://doi.org/10.1007s11207-015-0671-6.

Shen, C., Wang, Y., Pan, Z., Miao, B., Ye, P., Wang, S., 2014. Full-halo coronal mass ejections: arrival at the Earth. J. Geophys. Res. (Space Phys.) 119, 5107–5116. https://doi.org/10.1002/2014JA020001.

Smith, Z., Murtagh, W., Smithtro, C., 2004. Relationship between solar wind low-energy energetic ion enhancements and large geomagnetic storms. J. Geophys. Res. (Space Phys.) 109, A01110. https://doi.org/10.1029/2003JA010044.

Smith, Z.K., Murtagh, W.J., 2009. Solar wind low-energy energetic ion enhancements: a tool to forecast large geomagnetic storms. Adv. Space Res. 44, 775–788. https://doi.org/10.1016/j.asr.2009.06.018.

Srivastava, N., Venkatakrishnan, P., 2004. Solar and interplanetary sources of major geomagnetic storms during 1996–2002. J. Geophys. Res. (Space Phys.) 109, A10103. https://doi.org/10.1029/2003JA010175.

Temerin, M., Li, X., 2002. A new model for the prediction of Dst on the basis of the solar wind. J. Geophys. Res. (Space Phys.) 107, 1472. https://doi.org/10.1029/2001JA007532.

Temerin, M., Li, X., 2006. Dst model for 1995–2002. J. Geophys. Res. (Space Phys.) 111, A04221. https://doi.org/10.1029/2005JA011257.

Torsti, J., Valtonen, E., Lumme, M., et al., 1995. Energetic particle experiment (ERNE). Sol. Phys. 162, 505–531. https://doi.org/10.1007/BF00733438.

Tsurutani, B.T., Gonzalez, W.D., 1997. The Interplanetary causes of magnetic storms: a review. Washington DC Am. Geophys. Union Geophys. Monogr. Ser. 98, 77–89. https://doi.org/10.1029/GM098p0077.

Valtonen, E., Laitinen, T., Huttunen-Heikinmaa, K., 2005. Energetic particle signatures of geoeffective coronal mass ejections. Adv. Space Res. 36, 2295–2302. https://doi.org/10.1016/j.asr.2005.08.046.

Vasanth, V., Chen, Y., Kong, X.L., Wang, B., 2015. Investigation of the geoeffectiveness of CMEs associated with IP Type II radio bursts. Sol. Phys. 290, 1815–1826. https://doi.org/10.1007/s11207-015-0713-0.

Vršnak, B., Žic, T., Vrbanec, D., et al., 2013. Propagation of interplanetary coronal mass ejections: the drag-based model. Sol. Phys. 285, 295–315. https://doi.org/10.1007/s11207-012-0035-4.

Wang, Y.M., Ye, P.Z., Wang, S., Zhou, G.P., Wang, J.X., 2002. A statistical study on the geoeffectiveness of Earth-directed coronal mass ejections from March 1997 to December 2000. J. Geophys. Res. (Space Phys.) 107, 1340. https://doi.org/10.1029/2002JA009244.

Yermolaev, Y.I., Yermolaev, M.Y., 2006. Statistic study on the geomagnetic storm effectiveness of solar and interplanetary events. Adv. Space Res. 37, 1175–1181. https://doi.org/10.1016/j.asr.2005.03.130.

Zhang, J., Dere, K.P., Howard, R.A., Bothmer, V., 2003. Identification of solar sources of major geomagnetic storms between 1996 and 2000. Astrophys. J. 582, 520–533. https://doi.org/10.1086/344611.

Zhang, J., Richardson, I.G., Webb, D.F., et al., 2007a. Solar and interplanetary sources of major geomagnetic storms (Dst ⩽-100 nT) during 1996-2005. J. Geophys. Res. (Space Phys.) 112, A10102. https://doi.org/10.1029/2007JA012321.

Zhang, J., Richardson, I.G., Webb, D.F., et al., 2007b. Correction to "Solar and interplanetary sources of major geomagnetic storms (Dst ⩽-100 nT) during 1996-2005". J. Geophys. Res. (Space Phys.) 112, A12103. https://doi.org/10.1029/2007JA012891.